atmosphere

MDPI

Article

Size Distribution of Chemical Components of Particulate Matter in Lhasa

Jinglin Li [1,2], Jian Yao [1], He Zhou [1,2], Jie Liang [1,2], Zhuoga Deqing [3,*] and Wei Liu [1,2,*]

[1] Shanghai Institute of Applied Physics, Chinese Academy of Sciences, No. 2019 Jialuo Road, Jiading District, Shanghai 201800, China
[2] Shanghai Institute of Applied Physics, University of Chinese Academy of Sciences, No. 19(A) Yuquan Road, Shijingshan District, Beijing 100049, China
[3] Tibet Institute of Plateau Atmospheric Environmental Science, No. 2 North of Linkuo Road, Lhasa 850000, China
* Correspondence: deching123@aliyun.com (Z.D.); liuwei@sinap.ac.cn (W.L.)

Abstract: To explore the contributions of chemical components in the particulate matter in Lhasa, the size distribution characteristics of the chemical components, such as carbonaceous species (organic carbon, OC; elemental carbon, EC), water-soluble ions (NH_4^+, Cl^-, SO_4^{2-}, and NO_3^-) and trace elements (Na, Ca, Al, V, Cr, Mn, Fe, Co, Ni, Cu, Zn, K, Mg, and Pb), were investigated from August 2018 to May 2019. Principal component analysis (PCA) was also used to simulate the source of the particulate matter. The chemical components showed bimodal size distributions, except for Cu. The highest mass concentration of OC appeared at < 0.49 μm, and the second highest one existed at 1.5–3.0 μm in winter or at 3.0–7.2 μm in other seasons. The maximum concentrations of NH_4^+, Cl^-, SO_4^{2-}, and NO_3^- were at < 0.49 μm and peaked at 0.95–1.5 μm or > 3.0 μm. For seasonality, the concentrations of NO_3^- and SO_4^{2-} were considerably higher in summer and autumn; trace elements (except for Cu, Zn, V, and Ni), OC, and EC presented higher values during late autumn and winter. The ratio between OC and EC (4.15–33.80) indicated the existence of secondary pollution in Lhasa. The $[NO_3^-]$–$[SO_4^{2-}]$ ratios during summer and autumn exceeding 1 suggested that the currently predominant vehicle exhaust made a greater contribution to the aerosols. According to the results of a PCA, the main pollution sources of particulate matter in Lhasa were suspended dust, biomass burning, fossil fuel combustion, secondary pollution, and vehicular emissions.

Keywords: size distribution; water-soluble ions; OC–EC; trace elements; PCA; Lhasa

Citation: Li, J.; Yao, J.; Zhou, H.; Liang, J.; Deqing, Z.; Liu, W. Size Distribution of Chemical Components of Particulate Matter in Lhasa. *Atmosphere* **2023**, *14*, 339. https://doi.org/10.3390/atmos14020339

Academic Editor: Tania Martellini

Received: 19 November 2022
Revised: 16 December 2022
Accepted: 21 December 2022
Published: 8 February 2023

1. Introduction

Atmospheric particulate matter (PM) is a complex mixture of solid and liquid particles in the atmosphere. These complex mixtures have significant effects on human health, global climate change, and air quality. Those effects are closely related to their size distribution [1–3]. Element carbon (EC) severely impacts visibility and aggravates climate change [4], while organic carbon (OC) contains large amounts of toxic organic pollutants and heavy metals [5]. In addition to carbonaceous aerosols, inorganic species, which are predominantly in the forms of sulfate, ammonium, nitrate, and other basic ions [6,7], comprise 20–60% of the aerosol mass. Trace elements (TEs) make up a small proportion of PM but are significant owing to their toxicity [8,9].

Lhasa, the metropolis of the Tibet Autonomous Region, is in the Tibetan Plateau (TP) and has a unique atmospheric environment impacted by low vegetation coverage and high altitude [10,11]. Except for natural conditions, occasional industrial activities, massive religious activities (e.g., burning juniper) [8,9,12], and a special energy structure (e.g., burning yak dung) [13,14] differentiate the chemical and physical properties of aerosols among cities all over the world. Furthermore, Lhasa is suffering from a dramatic urbanization process with increasing motor vehicles and inflowing tourists [12,13,15,16]. Therefore, it has

drawn scientific attention and public concerns. One study [12] revealed the concentrations of trace elements and lead isotopes. Unexpectedly high levels of glyoxal and methylglyoxal were observed in Lhasa [17]. However, the information on the size distribution and seasonal/temporal variations in concentrations of trace elements (PM) in Lhasa is sparse.

In addition to the unique environment atmosphere in Lhasa, many studies [17–21] have discussed whether Lhasa's air pollution could be a pollutant source of TP. The trend in Lhasa differs greatly from those observed by a rapid increase of the Hg trend in the remote areas of the Tibetan Plateau [15]. Chen et al. [22] revealed the EFs of yak dung combustion aerosols and OC/BC values, suggesting that not all the BC of Nam Co was transported from South Asia. Size-segregated atmosphere PM sampling and analysis in TP cities are especially important in this regard. This kind of work could illuminate the characteristics of local emissions inside the TP, which are apparently meaningful for distinguishing the relative contributions from local vs. long-range transport [23].

In this study, the size-segregated atmosphere PM samples were collected in Lhasa. The concentrations and size distributions of OC, EC, water-soluble ions (WSIs), and TEs were determined. The principal component analysis (PCA) performed for the assessed chemical components (OC, EC, WSIs, and TEs) was used to identify the potential sources of atmospheric particulate matter and to provide an essential database for pollution source identification and environmental governance in TP.

2. Material and Methods

2.1. Sampling Sites and Samples Collection

Size-segregated particulate matter samples were collected on the rooftop, 18 m above ground level of the Tibet Meteorological Bureau (29°39′ N, 91°08′ E, 3679 m a.s.l.). The Bureau is in a commercial sector of Lhasa characterized by relatively high traffic. It is surrounded by residential buildings, schools, hospitals, passenger stations, and temples. The Potala Palace, Ramoche Temple, and other famous tourist attractions were on the south of the sampling site. Regarding industrial emission sources, a coal-fueled power plant and several cement plants were in the proximity of the sampling site (shown in Figure 1).

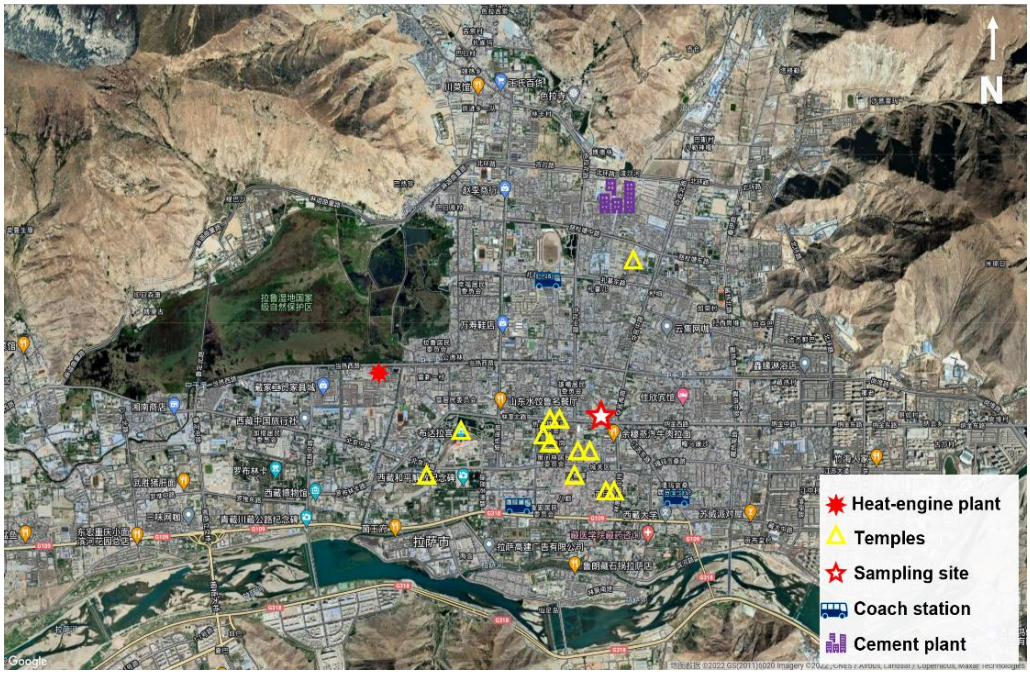

Figure 1. Location map of the sampling site (29°38′ N, 91°38′ E, 3679 m a.s.l.).

The samples were collected by a 5-stage high volume cascade impactor (Model 235, STAPLEX, New York, NY, USA). The flow rate of the instrument was calibrated to around 1.13 $m^3 \cdot min^{-1}$ before sampling. The equivalent aerodynamic cutoff diameters (D_p) of each stage were 0.49, 0.95, 1.5, 3.0, and 7.2 μm, respectively. In this study, the diameter of 3.0 μm was defined as the cutting point to distinguish fine particles from coarse particles. $PM_{3.0}$ corresponded to stages 1–4 (D_p = 0–3.0 μm) and $PM_{3\text{-}10}$ corresponded to stages 4–5 (D_p = 3.0–10 μm). The specific sampling time is shown in Figure A1. The sampling duration of each set sample was 144 h. Eventually, 96 size-segregated samples (16 sets) were successfully obtained. Figure A1 shows the sampling time and meteorological conditions.

2.2. Analytical Methods

The quartz fiber filters were heated in a muffle furnace at 800 °C for 4 h. Put quartz fiber filters in a dryer (temperature: 25 ± 0.5 °C; relative humidity: 40% ± 2%) for 48 h before weighing. After sampling, the samples were put in the same environment for 48 h. Filters were stood in the same conditions and weighed via a microbalance with sensitivity ± 0.01 Mg, to calculate the quality difference of the fiber filters before and after sampling. Subsequently, the samples were kept in a freezer (−20 °C) for analysis.

The sample filters with an area of 0.5025 cm^2 were cut and analyzed by Thermal/Optical Carbon Analyzer (DRI Model 2001A, Desert Research Institute, US) for OC and EC concentrations [24]. In this study, the IMPROVE_A temperature protocol heating program [22] was used. The bake program ran daily for removing the remaining impurities in the instrument cavity; the peak area was calibrated with the standard mixture of CH_4/CO_2 was passed into the Thermal/Optical Carbon Analyzer; the test was repeated for every 10 samples; and the results had a standard deviation of less than 5%.

A certain area of the sample filters was cut and extracted in 15 mL of ultrapure water (resistance: 18.2 MΩ-cm) by using ultrasonic vibration for 30 min [25]. After centrifugation, it was left to settle for 30 min. About 10 mL of the supernatant was filtered using nylon membrane filters (size: 0.22 μm), and then the extracted sample was stored in polypropylene sample bottles. The concentrations of inorganic ions (NH_4^+, Cl^-, SO_4^{2-}, and NO_3^-) were determined by using an ion chromatograph (ICS-2100, DIONEX, US).

Sample filters were placed in a PTFE (polytetrafluoroethylene) vessel digested with 6 mL HNO_3 (67%), 2 mL HCl (38%), and 0.4 mL HF (40%) at 150 °C for 3 h. After cooling, transfer the digestive solution to a volumetric flask and dilute it to 100 mL with ultrapure water. The elemental composition (Na, Ca, Al, V, Cr, Mn, Fe, Co, Ni, Cu, Zn, K, Mg, and Pb) was determined by using inductively coupled plasma mass spectrometry (X series 1 ICP–MS, US Thermo Fisher Company, Waltham, MA, US). Note that the levels of 4 species (U, Th, As, and Cd) in more than half of the size-segregated samples were lower than the detection limit of the ICP–MS [26].

2.3. Principal Component Analysis

Principal component analysis (PCA) is a multivariate statistical approach that is commonly used in environmental research. In this paper, PCA was performed for $PM_{3.0}$ and $PM_{3\text{-}10}$ data to identify possible sources in Lhasa. By assuming a linear relationship between the total mass concentration and the contributions of each species, the PCA factorized the data in numerous steps [27]. The PCA model is expressed as

$$Z_{ij} = \frac{C_{ij} - \overline{C}_j}{\sigma_j} = \sum_{k=1}^{p} g_{ik} h_{kj} \quad (1)$$

where $i = 1, \ldots, n$ samples; j replaces the concentrations of the OC, EC, Na, Ca, Al, V, Cr, Mn, Fe, Co, Ni, Cu, Zn, K, Mg, Pb, NH_4^+, Cl^-, SO_4^{2-}, and NO_3^- of the samples in the present study; $k = 1, \ldots, p$ pollution sources; g_{ik} and are the factor loadings and the factor sources; and $\overline{C}_j$ and σ_j are the arithmetic mean concentration and the standard deviation, respectively. This equation is solved by eigenvector decomposition.

3. Results and Discussion

3.1. PM and Carbon Fractions

3.1.1. Size Distribution and Temporal Variations

The size distribution of the atmospheric PM concentration in each season during the sampling period was shown (Figure 2). It exhibited typical bimodal distributions, with maxima (<0.49 μm) and smaller peaks (>7.2 μm) accounting for 51% and 21%, respectively. We suggested the high proportion of $PM_{0.49}$ because of the massive biomass burning (e.g., burning juniper and cow dung) and fossil fuel combustion in Lhasa [8]. The construction fugitive dust, suspended dust derived from the dry riverbed, and cement plant dust (Figure 1) were the main contributors to >7.2 μm [28,29]. The atmospheric PM concentration in different seasons varies greatly, with a descending order of winter > autumn > spring > summer, suggesting the worst air quality in winter. The meteorological conditions in winter were cold, and the central heating formed a stable thermal inversion layer [30], which weakened the potential for the dilution and diffusion of pollutants in the atmosphere.

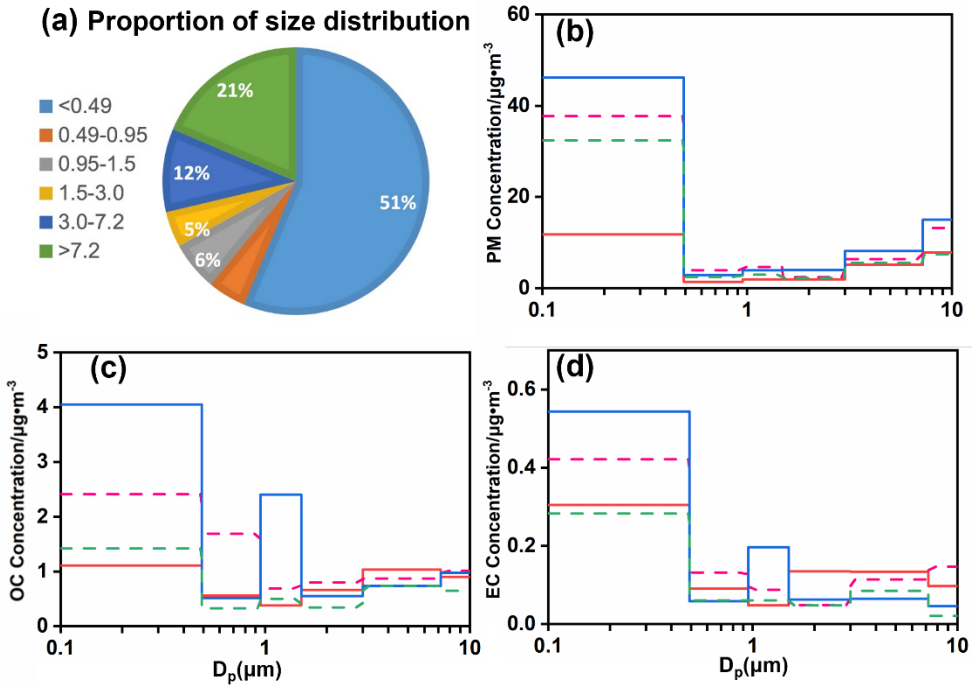

Figure 2. Concentration size distribution during different seasons: (**a**) proportion; (**b**) PM; (**c**) OC; and (**d**) EC. ((green line—spring, red line—summer, pink line—autumn and blue line—winter).

The size distribution of OC (Figure 2c) throughout the year appeared to have a relatively stable bimodal distribution. The highest level of OC mass concentration appeared at <0.49 μm; the second highest one existed in the PM, with the size ranging from 1.5 to 3.0 μm (winter) and 3.0 to 7.2 μm (except winter). We deduced that biomass burning (e.g., burning juniper and cow dung) generated a high concentration of OC at 0.49 μm [29]. One of the reasons for the OC peak at 3.0–7.2 μm is that suspended dust adsorbs some gases in volatile and semi-volatile compounds, and acts as a carrier for carbonaceous components. In addition, biological aerosols (e.g., pollen, micro-organisms, biological decay, and viruses) [31] and industry dust are others reasons for the OC concentration peak. The common contribution of multiple pollution sources corresponded to the OC−EC ratio at 3.0–7.2 μm for 0.51 in the following. Yan et al. [21] found that wet deposition rates of BC and WIOC peaked in summer and were affected mainly by the precipitation amount and emission strength of carbonaceous matter. The weak wet deposition effect [32] caused by the low relative humidity (21.21%) and precipitation (0.08 mm) in winter may be the reason why the second peak appears at 0.95–1.5 μm. Combined with the OC−EC ratio, we hypothesized that it resulted from incomplete combustion.

EC comes mainly from primary pollution sources such as vehicle exhaust, the incomplete combustion of coal, and biomass [16,33], which are basically smaller than 0.2 μm. Therefore, EC was distributed mainly in the PM smaller than 0.49 μm.

3.1.2. Secondary Aerosol Analysis

OC is divided into two parts: primary organic carbon (POC) and secondary organic carbon (SOC). The correlation of OC with EC can be used to judge the consistencies between the sources [34,35]. The strong correlation between OC and EC indicates a proximity to the sources. A strong correlation was obtained between OC and EC at 0.95–1.5 μm for 0.82, while poor correlations were obtained between OC and EC at < 0.49 μm, 0.49−0.95 μm, and 3.0–7.2 μm, indicating that OC has other sources, in addition to combustion sources, such as biological emissions, gas-particle conversion organic matter, etc. [36].

The ratio of OC to EC is an important diagnostic indicator to demonstrate emission sources, secondary organic aerosol (SOA) formation, and different removal rates [37]. When the ratio of OC to EC exceeds 2, it indicates the formation of SOC. The larger the OC−EC ratios, the higher the concentration of SOC [25,38]. The characteristic ranges of OC−EC rations for motor vehicle exhaust (1.0–4.2) [39], coal burning (2.5–10.5) [40], biomass combustion (3.8–13.2 and 16.8–40.0) [41], cater emissions (32.9–81.6) [42], and suspended dust (13.1) [43] were given in the previous studies. The OC−EC ratios are greater than 2, indicating secondary pollution formation in Lhasa, as shown in Figure 3. In comparison with the other studies, the OC−EC ratios in Lhasa and Shanghai [44] are relatively consistent, at < 0.49 μm, 0.49–0.95 μm, and 0.95–1.5 μm (Figure 4).

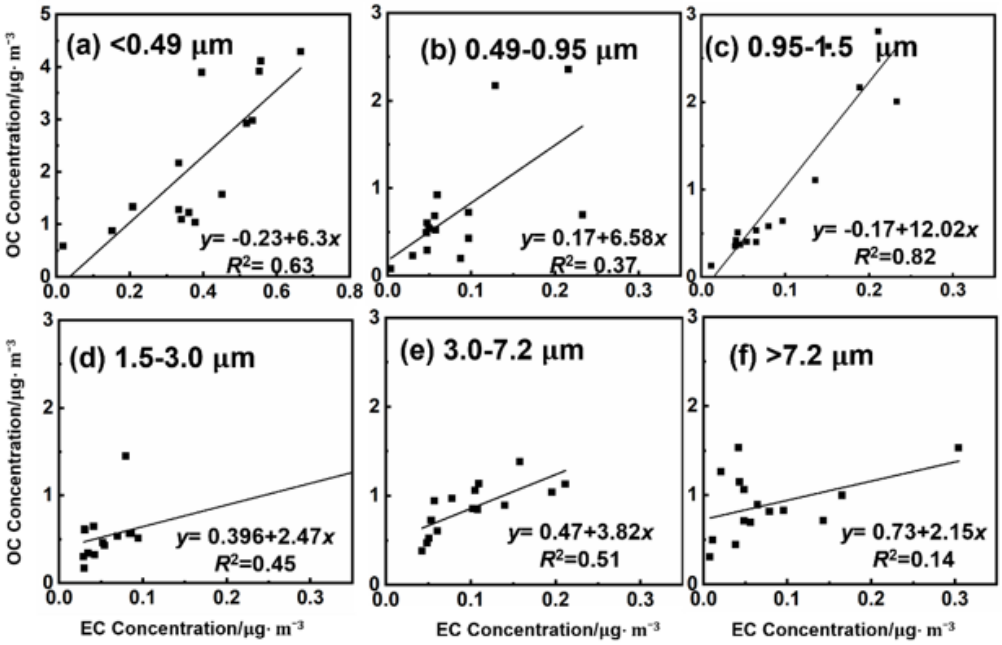

Figure 3. Correlation of OC and EC with particulate size in Lhasa (**a**–**f**).

However, even though the OC−EC ratios in Shanghai and Lhasa are similar, it is impossible to identify whether their sources are consistent, because of complex factors. The OC−EC ratios were around 7 in Shanghai at 3.0–7.2 μm and >7.2 μm, while they appeared at a higher ratio at >7.2 μm in Lhasa. This difference may be due to the stronger solar radiation over TP, which causes more SOC to be generated through photochemical reactions [45]. Aerosol-absorbing gas species and biogenic aerosols [46] increase OC concentrations. The lower contribution from EC and high contribution from secondary sources to OC result in higher OC−EC ratios at 3.0–7.2 μm and >7.2 μm in Lhasa [16].

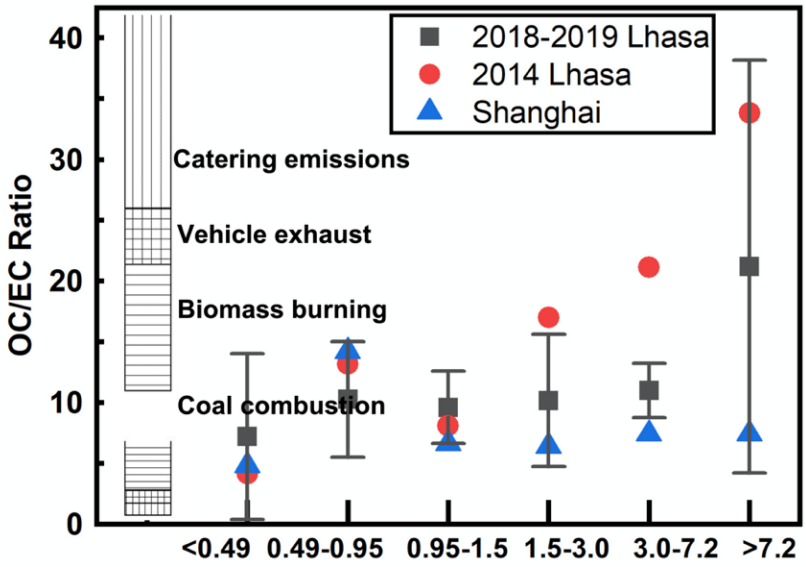

Figure 4. Comparison of OC−EC ratios of different particle sizes between Lhasa and Shanghai.

3.2. Water-Soluble Ions

3.2.1. Size Distribution and Temporal Variations

NH_4^+, Cl^-, SO_4^{2-}, and NO_3^- were the main water-soluble ions in PM in Lhasa [47]. Moreover, sulfates and nitrates in the atmosphere are more likely to come from the secondary conversion process [48], and we deduced stronger solar radiation causing more secondary pollution in Lhasa. The size distribution and seasonal variation of WSIs in Lhasa are shown in Figure 5. NH_4^+, Cl^-, SO_4^{2-}, and NO_3^- exhibited bimodal distributions: the concentration reached its maximum at <0.49 μm and peaked at 0.95−1.5 μm or >3.0 μm.

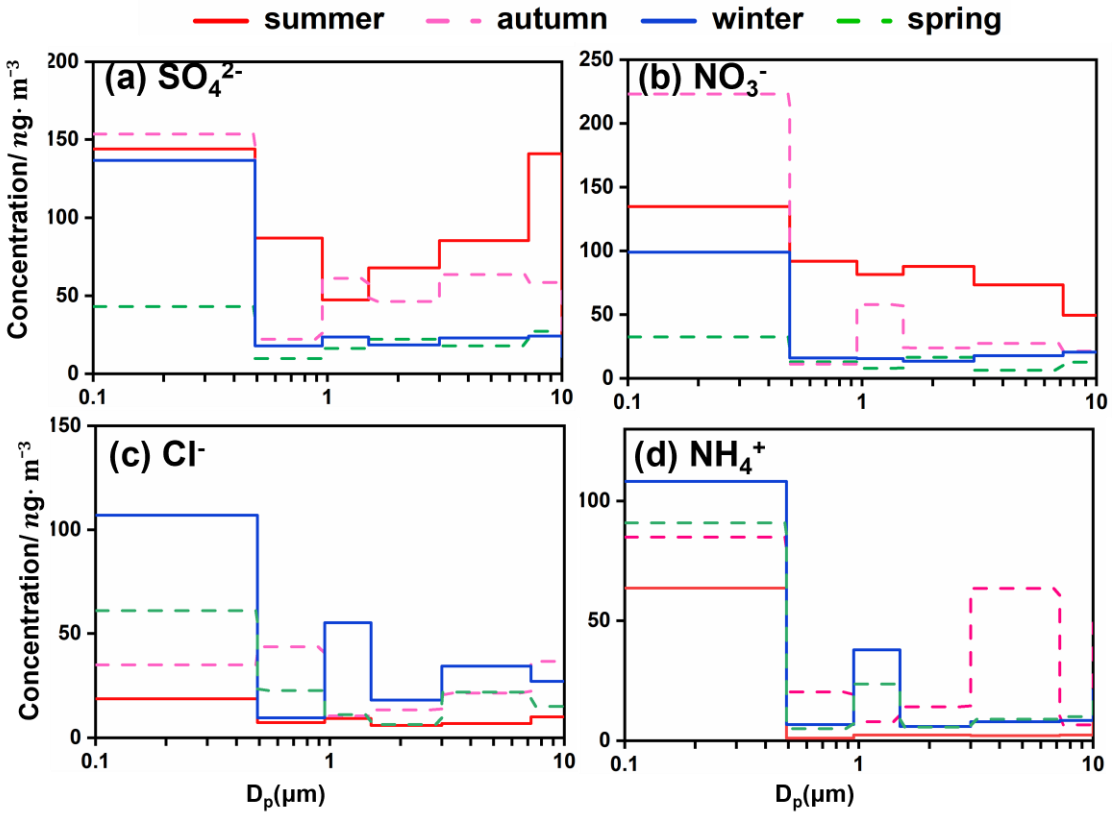

Figure 5. Concentration size distribution for WSIs during different seasons (**a**–**d**).

In addition to those in spring, the concentrations of SO_4^{2-} in the other three seasons were similar (<0.49 μm). The peaks of SO_4^{2-} concentration observed at < 0.49 μm may be due to coal-fired power plant emissions and the combustion of volatile sulfides in cement production [25] around the sampling point. A previous study in India showed that biomass burning could emit a wide variety of Cl^- [49]. In addition, cow dung is used for heating in winter, which emitted mainly OC, S, NH_4^+, and Cl^- [29]. Therefore, we deduced the concentration of NH_4^+ and Cl^- to reach the maximum in winter at 1.5−3 μm. Significantly, the concentration of SO_4^{2-} exhibited the peak at 3.0−7.2 μm or > 7.2μm (except summer), which may be due to excess soil dust from sparse vegetation and dried-up bed in the dry seasons. The concentrations of Cl^-, $NH_4^{+,}$ and SO_4^{2-} exhibited maxima in winter with a size of <0.49 μm. In contrast, theNO_3^- concentration exhibited its maximum in autumn and its peak in summer because of the main tourist seasons in Lhasa [12]. The increase of vehicle exhaust emissions is the most likely reason. Furthermore, NH_4NO_3 can be easily transformed into gaseous nitric acid, which could undergo a heterogeneous reaction in coarse particles [50,51]. However, the concentration of NO3$^-$ in summer was higher than in other seasons, except for the PM smaller than 0.49 μm.

3.2.2. $[NO_3^-]$–$[SO_4^{2-}]$

The $[NO_3^-]$−$[SO_4^{2-}]$ ratios in PM with different sizes in different seasons are given in Figure 6. It can be used to qualitatively compare the contribution of mobile and stationary sources to pollutants [52–54]. The larger the ratio, the greater the influence of mobile sources, such as vehicle exhaust. We found that the $[NO_3^-]$−$[SO_4^{2-}]$ ratio was higher than 1 at <0.49 μm and decreased with the increase of particle size in autumn. The $[NO_3^-]$− $[SO_4^{2-}]$ ratio was higher than 1 (except > 7.2 μm), and the reason for the high concentration of NO_3^- in the summer was mentioned above. Furthermore, the $[NO_3^-]$−$[SO_4^{2-}]$ ratio was lower than 1 in winter and spring (except 0.49–0.95 μm). The results suggested that in winter and spring, stationary sources contributed more pollutants than mobile sources.

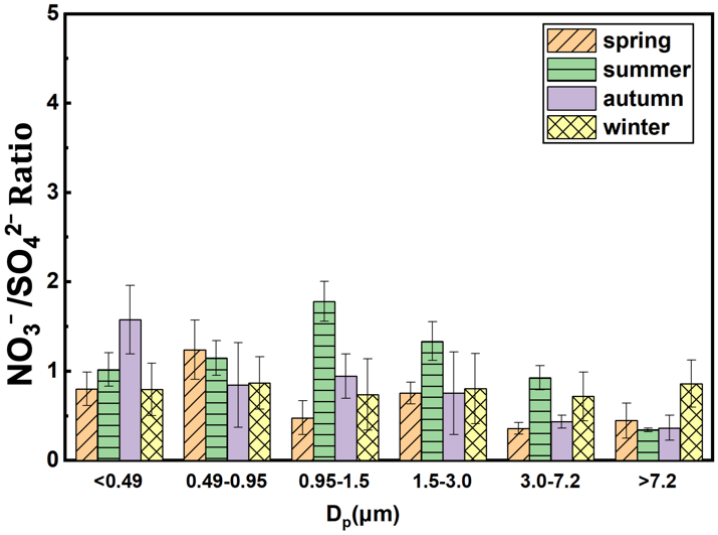

Figure 6. Size distribution of $[NO_3^-]$−$[SO_4^{2-}]$ ratio during different seasons.

3.3. Trace Elements

3.3.1. Trace Elements in Total Suspended Dust (TSP)

Among PM, Ca, Na, Al, Mg, K, and Fe were important crustal elements enriched in suspended dust [55]. Furthermore, the abundance of K was derived from biomass burning (existing as K_2SO_4 and KNO_3) [56]. Trace elements such as Cr, Cu, Cd, Mn, Ni, Zn, Pb, etc. with low concentrations had acute toxic and mutagenic effects on human health. Different regions and pollution sources led to regional differences in the size distributions and concentration of TEs in PM.

In this study, among the 14 trace elements, Al (1.86 ± 0.6 μg/m^3, 32.8%) was the most abundant species, followed by Fe (1.21 ± 0.4 μg/m^3, 21.3%), Ca (1.06 ± 0.35 μg/m^3, 18.8%), K (0.7 ± 0.4 μg/m^3, 12.4%), Na (0.35 ± 0.13 μg/m^3 6.3%), Mg (0.218 ± 0.07 μg/m^3, 3.8%), and Cu (0.21 ± 0.07 μg/m^3, 3.7%) in total metal concentration in TSP (Figure 7). These seven metal species constituted 99% of the total metal concentrations, whereas the other seven metal species constituted 1% of the metal concentration in TSP. The concentrations of As and Cd were close to zero; the concentrations of V and Cr were also negligible, which indicated that the heavy industry [57–59] was underdeveloped in Lhasa and that no smelter, boiler plant, or other production activities were near the sampling point.

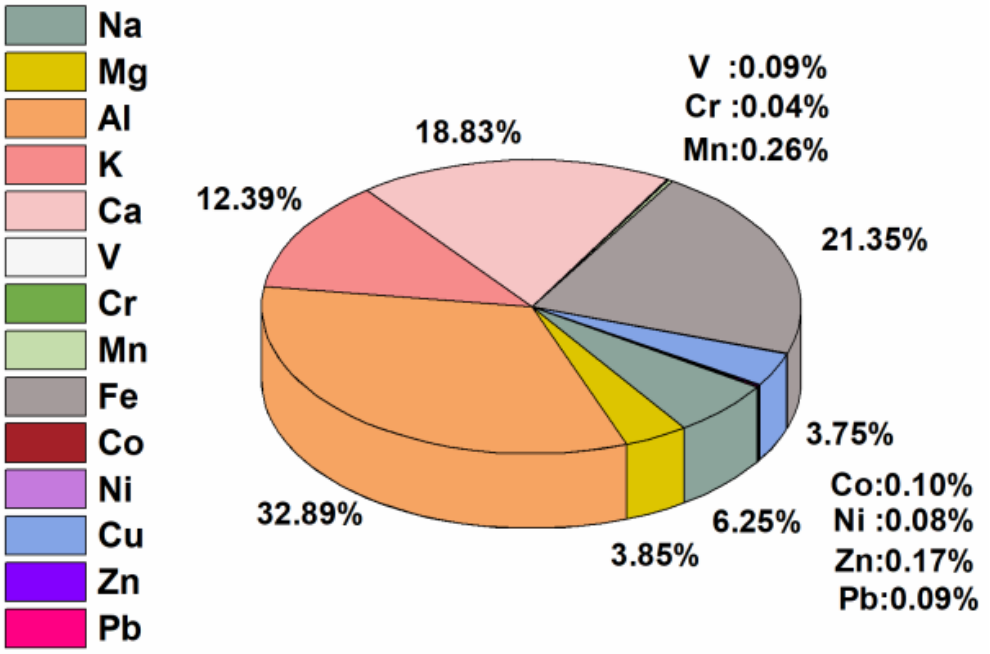

Figure 7. Proportion for the mass concentration of trace elements in PM in Lhasa.

Compared with other cities in China (Table A1), the mass concentrations of Mg, K, Mn, Cr, Ni, and Zn in PM_3 were lower than the representative locations of Sichuan, Beijing−Tianjin−Hebei region, the Yangtze River Delta, and northern industrial city−Chifeng in China. The mass concentrations of Al, Fe, and Ca were higher than those of Chifeng, Chengdu, and Chongqing and lower than the Beijing−Tianjin−Hebei region and the Jiangsu, Zhejiang, and Shanghai regions. Cu here was much higher than the amounts of Cu in other regions.

3.3.2. Size Distribution and Temporal Variations

Except for Co and Cr, the 12 trace elements were considered to be significant in this study, as shown in Figure 8. Na, Al, Mg, and K exhibited typical bimodal distributions with similar seasonal variations. These species exhibited maximal concentrations at <0.49 μm (in winter and spring) and >7.2 μm in summer (Figure 8). We inferred that the abundance of K smaller than <0.49 μm is from the biomass burning with wood and cow dung for heating [60,61]. Moreover, suspended soil contributed more in summer compared with biomass burning, where Na, Al, Mg, and K were important crustal elements [62].

Ca was a crustal element that came mainly from suspended dust, road dust, and building construction [29,63]. The mass distribution concentration of Ca was obtained from Figure 8f, which has two characteristics: (1) the highest peak was at >7.2 μm; (2) the concentration of Ca was similar in the four seasons at <0.49 μm, while it was higher in summer and autumn than in spring and winter at >7.2 μm. The reason for these two characteristics was that Ca originated mainly from coarse particles. In addition, the

main source of Ca, construction dust, contributed the least in winter and spring thanks to the bad weather conditions. In contrast, in summer and autumn, the remarkable correlations for Ca-Fe in coarse particles in winter and spring confirmed the above conclusion (Figure 9).

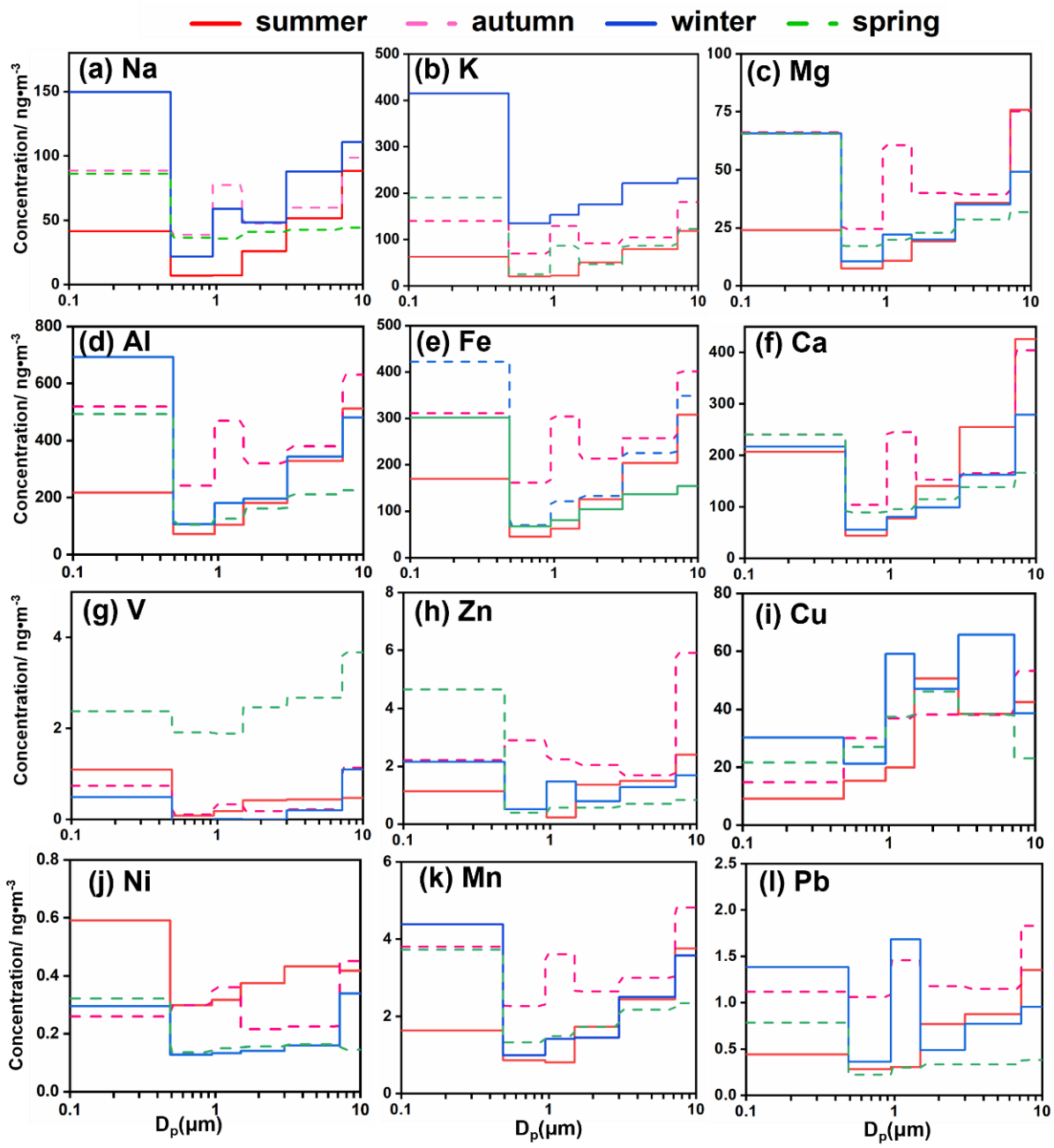

Figure 8. Concentration size distribution of trace elements during different seasons (**a**–**l**).

The element Fe included both anthropogenic sources, such as mining dust and construction building, and natural sources, such as barely Fe-rich soil [64]. It was observed that the mass distribution concentration of Fe presented two peaks, at< 0.49 μm and >7.2 μm. However, the changes during the seasons were slightly different. Apart from the effects of anthropogenic sources, climatic conditions such as low relative humidity and no rainfall (except summer) were beneficial for resuspended dust and soils [65,66].

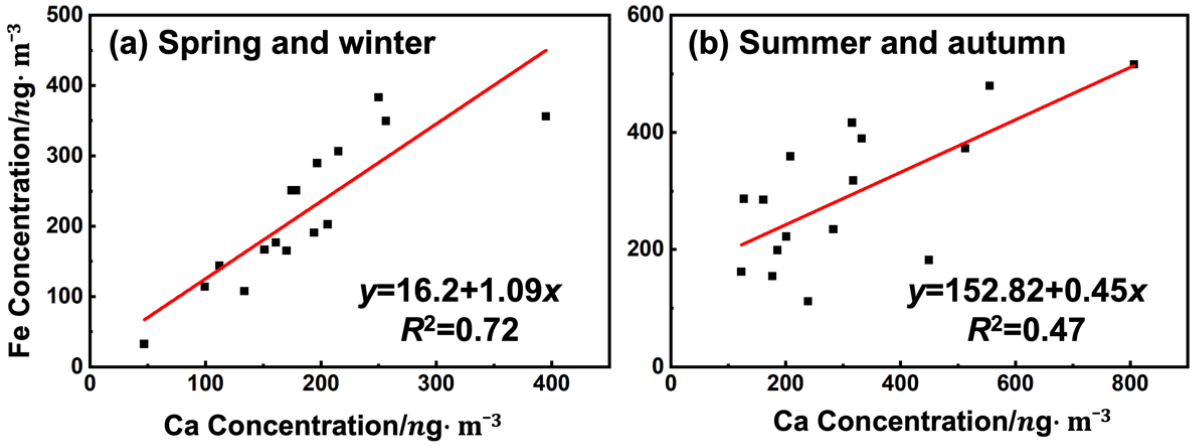

Figure 9. The correlation of Ca and Fe concentration ($PM_{3\text{-}10}$) during different seasons: (**a**) spring and winter; (**b**) summer and autumn;.

The mass distribution of Cu showed no obvious seasonal variation. The elevated Cu in winter might have been related to the more frequent occurrences of unfavorable dispersion conditions in cold periods [67]. The concentrations of As and Cd in PM in Lhasa were 0, which indicated that Cu did not originate from mineral smelting; meanwhile, when the sampling site was in the center of Lhasa with heavy traffic, Cu may have originated from the wear products of brake pads [68]. In addition, Tibet had many minerals for which suspended dust was an important contributor.

V and Ni were the two most abundant elements in petroleum that [69,70] related to the combustion emission of automobile fuel. Ni showed a higher concentration at < 0.49 μm in the autumn and summer (Figure 8), which was consistent with the seasonal variation of NO_3^- (Figure 5). V showed the highest concentration at all size distributions in spring, suggesting another source (except automobile exhaust) that we were not sure about.

Compared with Ni and V, Zn showed distinct seasonal patterns, suggesting more-complex sources [71–73]. It is observed that the mass distribution concentration of Zn presented two peaks, at 0.49 μm and > 7.2 μm. In addition, coal combustion may have been the reason for the high mass concentration of Pb in autumn and winter [74]. Previous studies [29] have shown that V, Ni, and Mn originated mainly from suspended dust, in Lhasa. Although we deduced the same source of these elements in coarse particles, the seasonal variation of their mass concentrations was higher in autumn and winter than in summer, at >7.2 μm.

3.4. Source Apportionment of PM in Lhasa

To understand and identify the possible sources of PM in Lhasa, PCA was performed for chemical constituents of $PM_{3.0}$ and $PM_{3.0\text{-}10}$ (OC, EC, Na, Ca, Al, V, Cr, Mn, Fe, Co, Ni, Cu, Zn, K, Mg, Pb, SO_4^{2-}, NO_3^-, NH_4^+, and Cl^-) by the varimax-rotated factor matrix method of the SPSS statistics viewer.

Table 1 summarizes the output of PCA for $PM_{3.0}$ data for Lhasa. The factor 1 source was identified, where the high loading of OC, EC, Pb, Mn, Ni, and Cu contributed to biomass burning and fossil fuel combustion with 37.31% variance. The high loading of OC and EC can be found in combustion emissions [75]. PC2 contained loading of Mg, Al, Ca, and V, which indicated the major contribution of suspended dust, as these also were crustal elements in fine particles [76]. PC3 was characterized by high ammonium, sulfate, and nitrate that could be identified as a mixture of secondary sulfate and secondary nitrate. Moreover, secondary sulfate and nitrate were divided into different principal components by factor methods, in some research. With 7.49% of the variance, PC4 contained only the high loading of Na and Co, whose sources were difficult to identify from the current data.

Table 1. PCA for TEs, WSIs, OC, and EC in PM_3 and $PM_{3\text{-}10}$.

Component	PM_3				$PM_{3\text{-}10}$				
	PC1	**PC2**	**PC3**	**PC4**	**PC1**	**PC2**	**PC3**	**PC4**	**PC5**
Na				−0.83	0.95	0.15	0.16		0.11
Mg	0.79	0.55			0.89	0.22	0.32		
Al	0.88	0.45			0.89	0.31	0.16	0.19	0.13
Ca	0.64	0.64	0.18	0.11	0.89		0.24		
K	0.46	0.81	−0.13		0.88	0.12	0.11	−0.11	−0.15
V		0.84			0.84	0.28	0.16		0.27
Cr	0.44	0.65	0.40		0.36	0.77	0.26	0.22	−0.20
Fe	0.84	0.48	0.14			0.75		−0.22	0.19
Mn	0.87	0.43			0.48	0.70		0.26	0.19
Co			−0.16	0.84	0.42	0.68	0.41		−0.28
Ni	0.61	0.70		−0.20	0.39	0.58	−0.34		0.17
Cu	0.61		−0.38	−0.12		0.56	0.20	0.56	−0.47
Zn	0.78		0.18		0.28		0.87		0.12
Pb	0.93	0.14			0.21	0.17	0.86		
Cl^-	0.20		0.80		0.21		0.81		0.19
NH_4^+		0.22	0.72	0.10			0.61		0.32
NO_3^-	0.16		0.91		0.30			0.92	
SO_4^{2-}			0.90		−0.21	0.16	−0.11	0.89	
OC	0.84		0.22						0.87
EC	0.73		0.39	0.22	0.22	0.16	0.26		0.68
Variance (%)	37.31	19.38	16.41	7.49	29.60	16.50	15.62	10.66	9.57
Cumulative variance (%)	37.31	56.69	73.10	80.60	29.60	46.10	61.72	72.38	81.95

Extraction method—principal component analysis; rotation method—varimax, eigenvalues > 1.0

The five factors in $PM_{3\text{-}10}$ were extracted as principal components, which accounted for 81.95% of the total variance. Source 1 was interpreted as suspended dust because of the high factor loadings for crustal elements, e.g., Al, Si, Ca, Fe, and Mg, in the PCA results [77]. PC2 was explained by vehicular emissions given that Cu, Ni and Zn were enriched with 16.5% of the variance [68]. The study showed that Zn and Cu were found in brake-wear emissions and some tailpipe emissions. Moreover, brake-wear particles were distributed in the entire size range larger than 1 μm, and more than 75% of particles were found in the coarse mode [72]. High factor loadings (PC3) for SO_4^{2-}, NO_3^-, and Cl^- were probably attributed to secondary aerosols. PC4 and PC5 may have been a mixture of coal combustion and biomass burning because of the high level of K, Ni, and OC, and a high level of K was found, indicating that biomass burning was occurring [78].

4. Conclusions

Understanding the contributions of chemical composition in Lhasa is crucial because of its distinctive geographical conditions and energy consumption structure. The characterization of OC, EC, WSIs, and TEs in the size-segregated aerosols in Lhasa was presented on the basis of a one-year sampling. Our major conclusions are listed below:

(1) Except for Cu, the size distributions of all the components were bimodal or multimodal. The highest level of OC mass concentration appeared at <0.49 μm, and the second highest one existed at 1.5–3.0 μm (winter) or 3.0–7.2 μm (except winter). EC was distributed mainly in the PM smaller than 0.49 μm. The ratio between OC and EC (4.15–33.80) indicated the existence of secondary pollution. The concentrations of NH_4^+, Cl^-, SO_4^{2-}, and NO_3^- reached their maxima at <0.49 μm and peaked at 0.95−1.5 μm or >3.0 μm.

(2) For seasonality, the concentrations of NO_3^- and SO_4^{2-} were considerably higher in summer and autumn; metal elements (except for Cu, Zn, V, and Ni), OC, and EC presented higher values during late autumn and winter. $[NO_3^-]$–$[SO_4^{2-}]$ ratios during summer and autumn exceeding 1 indicated that the currently predominant vehicle exhaust accounted for a greater contribution to the aerosols.

(3) In descending order of concentrations, Al, Fe, Ca, K, Na, Mg, and Cu were the seven trace elements that constituted 99% of TSP, whereas the other seven metal species constituted 1% of TSP. The concentrations of As and Cd were close to zero.

(4) A principal component analysis (PCA) was performed, which showed that the main pollution sources of $PM_{3.0}$ in Lhasa were biomass burning and fossil fuel combustion (37.31%), suspended dust (19.38%), and secondary pollution (16.41%). Suspended dust (29.6%), vehicular emissions (16.5%), secondary pollution (15.62%), biomass burning (1.66%), and coal combustion (9.57%) were the main contributors to $PM_{3\text{-}10}$ in Lhasa.

Author Contributions: Formal analysis, J.L. (Jie Liang).; Resources, Z.D.; Data curation, W.L.; Writing—original draft, J.L. (Jinglin Li); Writing—review & editing, H.Z.; Project administration, Z.D.; Funding acquisition, Z.D., J.Y. and W.L. All authors have read and agreed to the published version of the manuscript.

Funding: This research was funded by the National Natural Science Foundation of China (Grant Number: 11775180).

Informed Consent Statement: Informed consent was obtained from all subjects involved in the study.

Data Availability Statement: Not applicable.

Conflicts of Interest: The authors declare no conflict of interest.

Appendix A

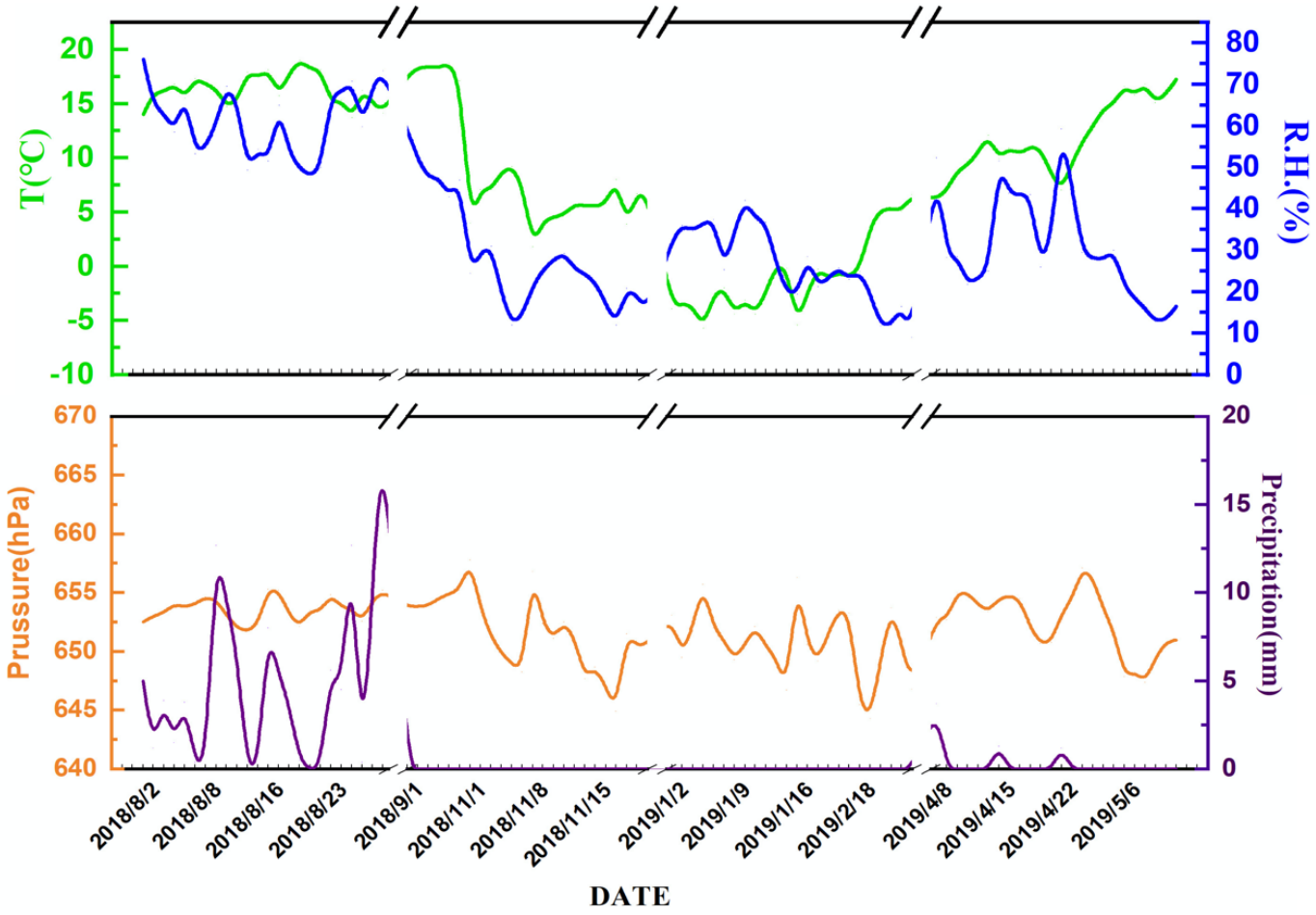

Figure A1. The characteristics of the meteorological parameters in Lhasa Station during sampling.

Table A1. Comparison of the mass concentrations of TEs (PM_3) with other cities in China.

Location	Periods	Mg	Al	K	Ca	Ti	V	Cr	Mn	Ni	Cu	Zn	Pb	Fe	Reference
								($ng \cdot m^{-3}$)							
Lhasa	2018–2019	122.8	1057	425.1	551.5	40.02	3.278	1.047	8.66	0.02	125.73	5.19	4.08	682	
Chifeng	2016–2017	168.9	547.3	1012	454.3	26.9	1.8	2.4	16.6	1.2	16.5	83.7	51	390	[79]
Chengdu	2014–2015	—	281	720	240	32.5	1.9	5.6	33.8	2.1	18.7	238	55.4	456	[80]
Beijing	2009–2010	600	970	1730	2420	40	3.3	19.9	72.6	7.5	44.3	113	50.4	586	
Tianjin		700	1170	2150	3280	40	4.9	13.4	102	7.3	138	324	142	1490	[65]
Nanjing	2013–2014	209	705	—	1520	—	9.88	13.2	—	9.3	24.7	746	220	2020	
Shanghai		298	922	—	1930	—	16.5	16.9	—	14.9	24.2	677	298	1840	[81]

References

1. Chow, J.C.; Watson, J.G.; Lowenthal, D.H.; Magliano, K.L. Size-Resolved Aerosol Chemical Concentrations at Rural and Urban Sites in Central California, USA. *Atmos. Res.* **2008**, *90*, 243–252. [CrossRef]
2. Pan, Y.; Tian, S.; Li, X.; Sun, Y.; Li, Y.; Wentworth, G.R.; Wang, Y. Trace Elements in Particulate Matter from Metropolitan Regions of Northern China: Sources, Concentrations and Size Distributions. *Sci. Total Environ.* **2015**, *537*, 9–22. [CrossRef] [PubMed]
3. Donaldson, K.; Brown, D.; Clouter, A.; Duffin, R.; Macnee, W.; Renwick, L.; Tran, L.; Stone, V. The Pulmonary Toxicology of Ultrafine Particles. *J. Aerosol Med.* **2002**, *15*, 213–220. [CrossRef] [PubMed]
4. Bond, T.C.; Doherty, S.J.; Fahey, D.W.; Forster, P.M.; Berntsen, T.; Deangelo, B.J.; Flanner, M.G.; Ghan, S.; Kärcher, B.; Koch, D.; et al. Bounding the Role of Black Carbon in the Climate System: A Scientific Assessment. *J. Geophys. Res. Atmos.* **2013**, *118*, 5380–5552. [CrossRef]
5. Bahadur, R.; Praveen, P.S.; Xu, Y.; Ramanathan, V. Solar Absorption by Elemental and Brown Carbon Determined from Spectral Observations. *Proc. Natl. Acad. Sci. USA* **2012**, *109*, 17366–17371. [CrossRef] [PubMed]
6. Kong, S.; Wen, B.; Chen, K.; Yin, Y.; Li, L.; Li, Q.; Yuan, L.; Li, X.; Sun, X. Ion Chemistry for Atmospheric Size-Segregated Aerosol and Depositions at an Offshore Site of Yangtze River Delta Region, China. *Atmos. Res.* **2014**, *147–148*, 205–226. [CrossRef]
7. Xu, J.; Wang, Z.; Yu, G.; Qin, X.; Ren, J.; Qin, D. Characteristics of Water Soluble Ionic Species in Fine Particles from a High Altitude Site on the Northern Boundary of Tibetan Plateau: Mixture of Mineral Dust and Anthropogenic Aerosol. *Atmos. Res.* **2014**, *143*, 43–56. [CrossRef]
8. Cui, L.; Duo, B.; Zhang, F.; Li, C.; Fu, H.; Chen, J. Physiochemical Characteristics of Aerosol Particles Collected from the Jokhang Temple Indoors and the Implication to Human Exposure. *Environ. Pollut.* **2018**, *236*, 992–1003. [CrossRef]
9. Kumar, P.; Kumar, S.; Yadav, S. Seasonal Variations in Size Distribution, Water-Soluble Ions, and Carbon Content of Size-Segregated Aerosols over New Delhi. *Environ. Sci. Pollut. Res.* **2018**, *25*, 6061–6078. [CrossRef]
10. Cong, Z.; Kang, S.; Liu, X.; Wang, G. Elemental Composition of Aerosol in the Nam Co Region, Tibetan Plateau, during Summer Monsoon Season. *Atmos. Environ.* **2007**, *41*, 1180–1187. [CrossRef]
11. Yang, R.; Zhang, S.; Li, A.; Jiang, G.; Jing, C. Altitudinal and Spatial Signature of Persistent Organic Pollutants in Soil, Lichen, Conifer Needles, and Bark of the Southeast Tibetan Plateau: Implications for Sources and Environmental Cycling. *Environ. Sci. Technol.* **2013**, *47*, 12736–12743. [CrossRef] [PubMed]
12. Cong, Z.; Kang, S.; Luo, C.; Li, Q.; Huang, J.; Gao, S.; Li, X. Trace Elements and Lead Isotopic Composition of PM10 in Lhasa, Tibet. *Atmos. Environ.* **2011**, *45*, 6210–6215. [CrossRef]
13. Duo, B.; Zhang, Y.; Kong, L.; Fu, H.; Hu, Y.; Chen, J.; Li, L.; Qiong, A. Individual Particle Analysis of Aerosols Collected at Lhasa City in the Tibetan Plateau. *J. Environ. Sci. China* **2015**, *29*, 165–177. [CrossRef] [PubMed]
14. Wei, N.; Wang, G.; Deng, K.; Feng, J.; Xiao, D.; Liu, W. Source Apportionment of Carbonaceous Particulate Matter during Haze Days in Shanghai Based on the Radiocarbon. *J. Radioanal. Nucl. Chem.* **2017**, *313*, 145–153. [CrossRef]
15. Huang, J.; Kang, S.; Tang, W.; He, M.; Guo, J.; Zhang, Q.; Yin, X.; Tripathee, L. Contrasting Changes in Long-Term Wet Mercury Deposition and Socioeconomic Development in the Largest City of Tibet. *Sci. Total Environ.* **2022**, *804*, 150124. [CrossRef]
16. Wan, X.; Kang, S.; Wang, Y.; Xin, J.; Liu, B.; Guo, Y.; Wen, T.; Zhang, G.; Cong, Z. Size Distribution of Carbonaceous Aerosols at a High-Altitude Site on the Central Tibetan Plateau (Nam Co Station, 4730ma.s.L.). *Atmos. Res.* **2015**, *153*, 155–164. [CrossRef]
17. Li, Q.; Gong, D.; Wang, H.; Wang, Y.; Han, S.; Wu, G.; Deng, S.; Yu, P.; Wang, W.; Wang, B. Rapid Increase in Atmospheric Glyoxal and Methylglyoxal Concentrations in Lhasa, Tibetan Plateau: Potential Sources and Implications. *Sci. Total Environ.* **2022**, *824*, 153782. [CrossRef]
18. Huang, J.; Kang, S.; Zhang, Q.; Guo, J.; Chen, P.; Zhang, G.; Tripathee, L. Atmospheric Deposition of Trace Elements Recorded in Snow from the Mt. Nyainqêntanglha Region, Southern Tibetan Plateau. *Chemosphere* **2013**, *92*, 871–881. [CrossRef]
19. Xia, X.; Zong, X.; Cong, Z.; Chen, H.; Kang, S.; Wang, P. Baseline Continental Aerosol over the Central Tibetan Plateau and a Case Study of Aerosol Transport from South Asia. *Atmos. Environ.* **2011**, *45*, 7370–7378. [CrossRef]
20. Niu, H.; He, Y.; Zhu, G.; Xin, H.; Du, J.; Pu, T.; Lu, X.; Zhao, G. Environmental Implications of the Snow Chemistry from Mt. Yulong, Southeastern Tibetan Plateau. *Quat. Int.* **2013**, *313–314*, 168–178. [CrossRef]
21. Yan, F.; Wang, P.; Kang, S.; Chen, P.; Hu, Z.; Han, X.; Sillanpää, M.; Li, C. High Particulate Carbon Deposition in Lhasa—A Typical City in the Himalayan-Tibetan Plateau Due to Local Contributions. *Chemosphere* **2020**, *247*, 125843. [CrossRef]

22. Chen, P.; Kang, S.; Bai, J.; Sillanpää, M.; Li, C. Yak Dung Combustion Aerosols in the Tibetan Plateau: Chemical Characteristics and Influence on the Local Atmospheric Environment. *Atmos. Res.* **2015**, *156*, 58–66. [CrossRef]
23. Wan, X.; Kang, S.; Xin, J.; Liu, B.; Wen, T.; Wang, P.; Wang, Y.; Cong, Z. Chemical Composition of Size-Segregated Aerosols in Lhasa City, Tibetan Plateau. *Atmos. Res.* **2016**, *174–175*, 142–150. [CrossRef]
24. Cao, J.J.; Wu, F.; Chow, J.C.; Lee, S.C.; Li, Y.; Chen, S.W.; An, Z.S.; Fung, K.K.; Watson, J.G.; Zhu, C.S.; et al. Characterization and Source Apportionment of Atmospheric Organic and Elemental Carbon during Fall and Winter of 2003 in Xi'an, China. *Atmos. Chem. Phys.* **2005**, *5*, 3127–3137. [CrossRef]
25. Wei, N.; Ma, C.; Liu, J.; Wang, G.; Liu, W.; Zhuoga, D.; Xiao, D.; Yao, J. Size-Segregated Characteristics of Carbonaceous Aerosols during the Monsoon and Non-Monsoon Seasons in Lhasa in the Tibetan Plateau. *Atmosphere* **2019**, *82*, 157. [CrossRef]
26. Pan, Y.; Wang, Y.; Sun, Y.; Tian, S.; Cheng, M. Size-Resolved Aerosol Trace Elements at a Rural Mountainous Site in Northern China: Importance of Regional Transport. *Sci. Total Environ.* **2013**, *461–462*, 761–771. [CrossRef]
27. Song, Y.; Xie, S.; Zhang, Y.; Zeng, L.; Salmon, L.G.; Zheng, M. Source Apportionment of PM2.5 in Beijing Using Principal Component Analysis/Absolute Principal Component Scores and UNMIX. *Sci. Total Environ.* **2006**, *372*, 278–286. [CrossRef]
28. Guo, Z.; Hao, Y.; Tian, H.; Bai, X.; Wu, B.; Liu, S.; Luo, L.; Liu, W.; Zhao, S.; Lin, S.; et al. Field Measurements on Emission Characteristics, Chemical Profiles, and Emission Factors of Size-Segregated PM from Cement Plants in China. *Sci. Total Environ.* **2022**, *818*, 151822. [CrossRef]
29. Hechen, Y.; Dan, Z.; Baolin, C.; Weidong, Z.; Pengchao, X.; Rui, Y.; Min, C.; Min, D.; Lei, J.; Xu, C.; et al. Establishment and Analysis of Atmospheric Particulate Matter Source Spectra in the Typical City of Lhasa, Qinghai-Tibetan Platea, China. *Environ. Monit. China* **2017**, *33*, 46–53.
30. Xinxin, A.; Zhao Yue, W.Q.J.N. Characteristics of Organic Carbon and Elemental Carbon in PM2.5 in Urban of Beijing. *Environ. Sci. Technol. Chinese* **2015**, *38*, 214–219. [CrossRef]
31. Bano, S.; Pervez, S.; Chow, J.C.; Matawle, J.L.; Watson, J.G.; Sahu, R.K.; Srivastava, A.; Tiwari, S.; Pervez, Y.F.; Deb, M.K. Coarse Particle (PM10–2.5) Source Profiles for Emissions from Domestic Cooking and Industrial Process in Central India. *Sci. Total Environ.* **2018**, *627*, 1137–1145. [CrossRef] [PubMed]
32. Shuiyuan, C.; Chao, L.; Lihui, H.; Yue, L.; Wang Zhijuan, T.C. Characteristics and Source Apportionment of Organic Carbon and Elemental Carbon in PM2.5 during the Heating Season in Beijing. *J. Beijing Univ. Technol.* **2014**, *40*, 586–591.
33. Hui, K.; Bin, Z.; Wang Honglei, S.S. Characterization and Variation of Organic Carbon (OC) and Elemental Carbon (EC) in PM2.5 during the Winter in the Yangtze River Delta Region, China. *Environ. Sci.* **2018**, *39*, 961–971.
34. Turpin, B.J.; Huntzicker, J.J. Secondary Formation of Organic Aerosol in the Los Angeles Basin: A Descriptive Analysis of Organic and Elemental Carbon Concentrations. *Atmos. Environ. Part A Gen. Top.* **1991**, *25*, 207–215. [CrossRef]
35. Cachier, H. Isotopic Characterization of Carbonaceous Aerosols. *Aerosol Sci. Technol.* **1989**, *10*, 379–385. [CrossRef]
36. Dai, Q.; Bi, X.; Liu, B.; Li, L.; Ding, J.; Song, W.; Bi, S.; Schulze, B.C.; Song, C.; Wu, J.; et al. Chemical Nature of PM2.5 and PM10 in Xi'an, China: Insights into Primary Emissions and Secondary Particle Formation. *Environ. Pollut.* **2018**, *240*, 155–166. [CrossRef]
37. Pio, C.; Cerqueira, M.; Harrison, R.M.; Nunes, T.; Mirante, F.; Alves, C.; Oliveira, C.; Sanchez de la Campa, A.; Artíñano, B.; Matos, M. OC/EC Ratio Observations in Europe: Re-Thinking the Approach for Apportionment between Primary and Secondary Organic Carbon. *Atmos. Environ.* **2011**, *45*, 6121–6132. [CrossRef]
38. Chow, J.C.; Watson, J.G.; Lu, Z.; Lowenthal, D.H.; Frazier, C.A.; Solomon, P.A.; Thuillier, R.H.; Magliano, K. Descriptive Analysis of PM2.5 and PM10 at Regionally Representative Locations during SJVAQS/AUSPEX. *Atmos. Environ.* **1996**, *30*, 2079–2112. [CrossRef]
39. Schauer, J.J.; Kleeman, M.J.; Cass, G.R.; Simoneit, B.R.T. Measurement of Emissions from Air Pollution Sources. 2. C1 through C30 Organic Compounds from Medium Duty Diesel Trucks. *Environ. Sci. Technol.* **1999**, *33*, 1578–1587. [CrossRef]
40. Chen, Y.; Zhi, G.; Feng, Y.; Fu, J.; Feng, J.; Sheng, G.; Simoneit, B.R.T. Measurements of Emission Factors for Primary Carbonaceous Particles from Residential Raw-Coal Combustion in China. *Geophys. Res. Lett.* **2006**, *33*, L20815. [CrossRef]
41. Schauer, J.J.; Kleeman, M.J.; Cass, G.R.; Simoneit, B.R.T. Measurement of Emissions from Air Pollution Sources. 3. C1-C29 Organic Compounds from Fireplace Combustion of Wood. *Environ. Sci. Technol.* **2001**, *35*, 1716–1728. [CrossRef] [PubMed]
42. He, L.Y.; Hu, M.; Huang, X.F.; De Yu, B.; Zhang, Y.H.; Liu, D.Q. Measurement of Emissions of Fine Particulate Organic Matter from Chinese Cooking. *Atmos. Environ.* **2004**, *38*, 6557–6564. [CrossRef]
43. Watson, J.G.; Chow, J.C.; Lu, Z.; Fujita, E.M.; Lowenthal, D.H.; Lawson, D.R.; Ashbaugh, L.L. Chemical Mass Balance Source Apportionment of PM10 during the Southern California Air Quality Study. *Aerosol Sci. Technol.* **1994**, *21*, 1–36. [CrossRef]
44. Zeng, G.W.Y.; Yao, J. Source Apportionment of Atmospheric Carbonaceous Particulate Matter Based on the Radiocarbon. *J. Radioanal. Nucl. Chem.* **2013**, *295*, 1545–1552. [CrossRef]
45. Cong, Z.; Kang, S.; Kawamura, K.; Liu, B.; Wan, X.; Wang, Z.; Gao, S.; Fu, P. Carbonaceous Aerosols on the South Edge of the Tibetan Plateau: Concentrations, Seasonality and Sources. *Atmos. Chem. Phys.* **2015**, *15*, 1573–1584. [CrossRef]
46. Seinfeld, J.H.; Pandis, S.N. Atmospheric Chemistry and Physics from Air Pollution to Climate Change Second Edition. *Environ. Sci. Policy Sustain. Dev.* **1998**, *40*, 26. [CrossRef]
47. Wei, N.; Xu, Z.; Liu, J.; Wang, G.; Liu, W.; Zhuoga, D.; Xiao, D.; Yao, J. Characteristics of Size Distributions and Sources of Water-Soluble Ions in Lhasa during Monsoon and Non-Monsoon Seasons. *J. Environ. Sci. China* **2019**, *82*, 155–168. [CrossRef]

48. Yukun, C.; Tianxue, W.; Xiaoling, Z.; Ruirui, S.; Xinrui, W.; Anan, L.; Guangjing, L.; Yongxiang, M.; Zirui, L.X.J. Component and Sources Analyses of PM2.5 in Typical Agricultural Regions of North China. *Chin. J. Atmosphreic Sci.* **2021**, *45*, 819–832. (in Chinese). [CrossRef]
49. Pavuluri, C.M.; Kawamura, K.; Swaminathan, T. Water-Soluble Organic Carbon, Dicarboxylic Acids, Ketoacids, and α-Dicarbonyls in the Tropical Indian Aerosols. *J. Geophys. Res. Atmos.* **2010**, *115*, D11302. [CrossRef]
50. Jun Li, J.; Hui Wang, G.; Ming Wang, X.; Ji Cao, J.; Sun, T.; Lei Cheng, C.; Jing Meng, J.; Feng Hu, T.A.; Xin Liu, S. Abundance, Composition and Source of Atmospheric PM 2.5 at a Remote Site in the Tibetan Plateau, China. *Tellus B Chem. Phys. Meteorol.* **2013**, *65*, 20281. [CrossRef]
51. Pathak, R.K.; Wang, T.; Wu, W.S. Nighttime Enhancement of PM2.5 Nitrate in Ammonia-Poor Atmospheric Conditions in Beijing and Shanghai: Plausible Contributions of Heterogeneous Hydrolysis of N_2O_5 and HNO_3 Partitioning. *Atmos. Environ.* **2011**, *45*, 1183–1191. [CrossRef]
52. Arimoto, R.; Duce, R.A.; Savoie, D.L.; Prospero, J.M.; Talbot, R.; Cullen, J.D.; Tomza, U.; Lewis, N.F.; Ray, B.J. Relationships among Aerosol Constituents from Asia and the North Pacific during PEM-West A. *J. Geophys. Res. Atmos.* **2011**, *101*, 2011–2023.
53. Calvo, A.I.; Alves, C.; Castro, A.; Pont, V.; Vicente, A.M.; Fraile, R. Research on Aerosol Sources and Chemical Composition: Past, Current and Emerging Issues. *Atmos. Res* **2013**, *120–121*, 1–28. [CrossRef]
54. Ho, K.F.; Lee, S.C.; Chow, J.C.; Watson, J.G. Characterization of PM10 and PM2.5 Source Profiles for Fugitive Dust in Hong Kong. *Atmos. Environ.* **2003**, *37*, 1023–1032. [CrossRef]
55. Sharma, S.K.; Mandal, T.K.; Saxena, M.; Rashmi; Rohtash; Sharma, A.; Gautam, R. Source Apportionment of PM10 by Using Positive Matrix Factorization at an Urban Site of Delhi, India. *Urban Clim.* **2014**, *10*, 656–670. [CrossRef]
56. Li, W.J.; Shao, L.Y.; Buseck, P.R. Haze Types in Beijing and the Influence of Agricultural Biomass Burning. *Atmos. Chem. Phys.* **2010**, *10*, 8119–8130. [CrossRef]
57. Dai, Q.L.; Bi, X.H.; Wu, J.H.; Zhang, Y.F.; Wang, J.; Xu, H.; Yao, L.; Jiao, L.; Feng, Y.C. Characterization and Source Identification of Heavy Metals in Ambient PM10 and PM2.5 in an Integrated Iron and Steel Industry Zone Compared with a Background Site. *Aerosol Air Qual. Res.* **2015**, *15*, 875–887. [CrossRef]
58. Moreno, T.; Alastuey, A.; Querol, X.; Font, O.; Gibbons, W. The Identification of Metallic Elements in Airborne Particulate Matter Derived from Fossil Fuels at Puertollano, Spain. *Int. J. Coal Geol.* **2007**, *71*, 122–128. [CrossRef]
59. Tian, H.Z.; Lu, L.; Hao, J.M.; Gao, J.J.; Cheng, K.; Liu, K.Y.; Qiu, P.P.; Zhu, C.Y. A Review of Key Hazardous Trace Elements in Chinese Coals: Abundance, Occurrence, Behavior during Coal Combustion and Their Environmental Impacts. *Energy Fuels* **2013**, *27*, 601–614. [CrossRef]
60. Wang, G.H.; Zhou, B.H.; Cheng, C.L.; Cao, J.J.; Li, J.J.; Meng, J.J.; Tao, J.; Zhang, R.J.; Fu, P.Q. Impact of Gobi Desert Dust on Aerosol Chemistry of Xi'an, Inland China during Spring 2009: Differences in Composition and Size Distribution between the Urban Ground Surface and the Mountain Atmosphere. *Atmos. Chem. Phys.* **2013**, *13*, 819–835. [CrossRef]
61. Ordou, N.; Agranovski, I.E. Mass Distribution and Elemental Analysis of the Resultant Atmospheric Aerosol Particles Generated in Controlled Biomass Burning Processes. *Atmos. Res.* **2017**, *198*, 108–112. [CrossRef]
62. Zhao, S.; Tian, H.; Luo, L.; Liu, H.; Wu, B.; Liu, S.; Bai, X.; Liu, W.; Liu, X.; Wu, Y.; et al. Temporal Variation Characteristics and Source Apportionment of Metal Elements in PM2.5 in Urban Beijing during 2018–2019. *Environ. Pollut.* **2021**, *268*, 115856. [CrossRef] [PubMed]
63. Yadav, S.; Tandon, A.; Tripathi, J.K.; Yadav, S.; Attri, A.K. Statistical Assessment of Respirable and Coarser Size Ambient Aerosol Sources and Their Timeline Trend Profile Determination: A Four Year Study from Delhi. *Atmos. Pollut. Res.* **2016**, *7*, 190–200. [CrossRef]
64. Sylvestre, A.; Mizzi, A.; Mathiot, S.; Masson, F.; Jaffrezo, J.L.; Dron, J.; Mesbah, B.; Wortham, H.; Marchand, N. Comprehensive Chemical Characterization of Industrial PM2.5 from Steel Industry Activities. *Atmos. Environ.* **2017**, *152*, 180–190. [CrossRef]
65. Zhao, P.S.; Dong, F.; He, D.; Zhao, X.J.; Zhang, X.L.; Zhang, W.Z.; Yao, Q.; Liu, H.Y. Characteristics of Concentrations and Chemical Compositions for PM2.5 in the Region of Beijing, Tianjin, and Hebei, China. *Atmos. Chem. Phys.* **2013**, *13*, 4631–4644. [CrossRef]
66. Zhao, H.; Che, H.; Zhang, X.; Ma, Y.; Wang, Y.; Wang, H.; Wang, Y. Characteristics of Visibility and Particulate Matter (PM) in an Urban Area of Northeast China. Atmos. *Pollut. Res.* **2013**, *4*, 427–434. [CrossRef]
67. Zhang, Y.L.; Cao, F. Fine Particulate Matter (PM 2.5) in China at a City Level. *Sci. Rep.* **2015**, *5*, 14884. [CrossRef]
68. Lin, Y.C.; Tsai, C.J.; Wu, Y.C.; Zhang, R.; Chi, K.H.; Huang, Y.T.; Lin, S.H.; Hsu, S.C. Characteristics of Trace Metals in Traffic-Derived Particles in Hsuehshan Tunnel, Taiwan: Size Distribution, Potential Source, and Fingerprinting Metal Ratio. *Atmos. Chem. Phys.* **2015**, *15*, 4117–4130. [CrossRef]
69. Venter, A.D.; Van Zyl, P.G.; Beukes, J.P.; Josipovic, M.; Hendriks, J.; Vakkari, V.; Laakso, L. Atmospheric Trace Metals Measured at a Regional Background Site (Welgegund) in South Africa. *Atmos. Chem. Phys.* **2017**, *17*, 4251–4263. [CrossRef]
70. Cui, X.; Zhou, T.; Shen, Y.; Rong, Y.; Zhang, Z.; Liu, Y.; Xiao, L.; Zhou, Y.; Li, W.; Chen, W. Different Biological Effects of PM 2.5 from Coal Combustion, Gasoline Exhaust and Urban Ambient Air Relate to the PAH/Metal Compositions. *Environ. Toxicol. Pharmacol.* **2019**, *69*, 120–128. [CrossRef]
71. Font, A.; de Hoogh, K.; Leal-Sanchez, M.; Ashworth, D.C.; Brown, R.J.C.; Hansell, A.L.; Fuller, G.W. Using Metal Ratios to Detect Emissions from Municipal Waste Incinerators in Ambient Air Pollution Data. *Atmos. Environ.* **2015**, *113*, 177–186. [CrossRef]

72. Bukowiecki, N.; Lienemann, P.; Hill, M.; Figi, R.; Richard, A.; Furger, M.; Rickers, K.; Falkenberg, G.; Zhao, Y.; Cliff, S.S.; et al. Real-World Emission Factors for Antimony and Other Brake Wear Related Trace Elements: Size-Segregated Values for Light and Heavy Duty Vehicles. *Environ. Sci. Technol.* **2009**, *43*, 8072–8078. [CrossRef] [PubMed]
73. Querol, X.; Viana, M.; Alastuey, A.; Amato, F.; Moreno, T.; Castillo, S.; Pey, J.; de la Rosa, J.; de la Campa, A.S.; Artíñano, B.; et al. Source Origin of Trace Elements in PM from Regional Background, Urban and Industrial Sites of Spain. *Atmos. Environ.* **2007**, *41*, 7219–7231. [CrossRef]
74. Jain, S.; Sharma, S.K.; Vijayan, N.; Mandal, T.K. Seasonal Characteristics of Aerosols (PM2.5 and PM10) and Their Source Apportionment Using PMF: A Four Year Study over Delhi, India. *Environ. Pollut.* **2020**, *262*, 114337. [CrossRef]
75. Zheng, M.; Salmon, L.G.; Schauer, J.J.; Zeng, L.; Kiang, C.S.; Zhang, Y.; Cass, G.R. Seasonal Trends in PM2.5 Source Contributions in Beijing, China. *Atmos. Environ.* **2005**, *39*, 3967–3976. [CrossRef]
76. Xie, M.; Feng, W.; He, S.; Wang, Q. Seasonal Variations, Temperature Dependence, and Sources of Size-Resolved PM Components in Nanjing, East China. *J. Environ. Sci. China* **2022**, *121*, 175–186. [CrossRef]
77. Gupta, P.; Satsangi, M.; Satsangi, G.P.; Jangid, A.; Liu, Y.; Pani, S.K.; Kumar, R. Exposure to Respirable and Fine Dust Particle over North-Central India: Chemical Characterization, Source Interpretation, and Health Risk Analysis. *Environ. Geochem. Health* **2020**, *42*, 2081–2099. [CrossRef]
78. Rahman, M.M.; Begum, B.A.; Hopke, P.K.; Nahar, K.; Thurston, G.D. Assessing the PM2.5 Impact of Biomass Combustion in Megacity Dhaka, Bangladesh. *Environ. Pollut.* **2020**, *264*, 114798. [CrossRef]
79. Hao, Y.; Meng, X.; Yu, X.; Lei, M.; Li, W.; Shi, F.; Yang, W.; Zhang, S.; Xie, S. Characteristics of Trace Elements in PM2.5 and PM10 of Chifeng, Northeast China: Insights into Spatiotemporal Variations and Sources. *Atmos. Res.* **2018**, *213*, 550–561. [CrossRef]
80. Wang, H.; Qiao, B.; Zhang, L.; Yang, F.; Jiang, X. Characteristics and Sources of Trace Elements in PM2.5 in Two Megacities in Sichuan Basin of Southwest China. *Environ. Pollut.* **2018**, *242*, 1577–1586. [CrossRef]
81. Ming, L.; Jin, L.; Li, J.; Fu, P.; Yang, W.; Liu, D.; Zhang, G.; Wang, Z.; Li, X. PM2.5 in the Yangtze River Delta, China: Chemical Compositions, Seasonal Variations, and Regional Pollution Events. *Environ. Pollut.* **2017**, *223*, 200–212. [CrossRef] [PubMed]